



Bromophenol blue degradation by contact-electro-catalysis[☆]

Shaoxin Li^{a,b,c}, Han Qian^{a,b}, Jinheng Xu^c, Zhong Lin Wang^{a,d,**}, Richard N. Zare^{c,*}, Di Wei^{a,*}

^a Beijing Institute of Nanoenergy and Nanosystems, Chinese Academy of Sciences, Beijing 101400, PR China

^b School of Nanoscience and Engineering, University of Chinese Academy of Sciences, Beijing 100049, PR China

^c Department of Chemistry, Stanford University, Stanford, CA 94305, USA

^d Beijing Key Laboratory of Micro-Nano Energy and Sensor, Center for High-Entropy Energy and Systems, Beijing Institute of Nanoenergy and Nanosystems, Chinese Academy of Sciences, Beijing 101400, PR China

ARTICLE INFO

Keywords:

Bromophenol blue
Dye degradation
Contact-electro-catalysis
Contact electrification
electron transfer

ABSTRACT

Bromophenol blue (BPB) is a widely used sulfonephthalein dye whose halogenated aromatic framework and high chemical stability confer strong environmental persistence and resistance to conventional degradation pathways. Herein, we report a contact-electro-catalysis (CEC) approach for the efficient degradation of BPB in aqueous media without the use of conventional catalysts like precious metals. Continuous solid-liquid contact electrification between polytetrafluoroethylene (PTFE) powder and water, driven by ultrasonication, induces interfacial electron transfer and radical generation, enabling oxidative dye degradation without the application of an external voltage. Time-resolved UV-vis spectroscopy reveals rapid discoloration and degradation of BPB across a broad pH range. Mass spectrometric analysis confirms a stepwise degradation process involving oxidized intermediates and low-molecular-weight fragments. Comprehensive structural and spectroscopic characterization demonstrates that PTFE remains chemically and structurally stable throughout the reaction, establishing CEC as a sustainable and effective way for the degradation of persistent halogenated dyes and underscores its broader potential for green pollutant remediation and molecular transformation.

1. Introduction

Synthetic dyes constitute a major class of persistent organic pollutants in aquatic environments, arising from their extensive use in chemical, biomedical and industrial processes [1]. Their complex aromatic frameworks, often reinforced by halogenation and heteroatom linkages, confer high chemical stability and vivid optical properties, but simultaneously hinder natural attenuation through hydrolysis, photodegradation, and biodegradation. As a result, dye-contaminated wastewater poses sustained ecological and toxicological risks, including light penetration inhibition, bioaccumulation, and adverse effects on aquatic organisms, while remaining difficult to treat using conventional wastewater remediation technologies [2,3]. Bromophenol blue (BPB), whose structure is shown in Fig. 1a, is a representative sulfonephthalein dye that has been widely employed as a pH indicator, tracking dye, and analytical probe owing to its sharp color transition, high molar

absorptivity, and exceptional chemical stability [4,5]. Its brominated aromatic framework and sulfone linkage, while essential for functional reliability in laboratory and industrial applications, also render BPB highly resistant to hydrolysis, photolysis, and microbial degradation [6,7]. Consequently, once released into aqueous systems, BPB exhibits pronounced environmental persistence and potential ecological toxicity [8]. Developing efficient and sustainable strategies for the degradation of BPB therefore not only addresses the remediation of a widely used halogenated dye, but also provides a model platform for tackling structurally robust dye pollutants more broadly.

Current approaches for BPB degradation mainly rely on advanced oxidation processes (AOPs), photocatalysis, electrochemical oxidation, and Fenton-type reactions [9–11]. Although these methods can partially decompose BPB, they often require external electrical bias, noble or transition-metal catalysts, or strong chemical oxidants. In addition, such processes may suffer from high operational costs, secondary pollution,

[☆] This article is part of a Special issue entitled: '20th ISEAC' published in Journal of Electroanalytical Chemistry.

* Corresponding authors.

** Corresponding author at: Beijing Key Laboratory of Micro-Nano Energy and Sensor, Center for High-Entropy Energy and Systems, Beijing Institute of Nanoenergy and Nanosystems, Chinese Academy of Sciences, Beijing 101400, PR China.

E-mail addresses: zlwang@binn.cas.cn (Z.L. Wang), rnz@stanford.edu (R.N. Zare), weidi@binn.cas.cn (D. Wei).

<https://doi.org/10.1016/j.jelechem.2026.119942>

Received 9 January 2026; Received in revised form 3 February 2026; Accepted 8 February 2026

Available online 16 February 2026

1572-6657/© 2026 Elsevier B.V. All rights are reserved, including those for text and data mining, AI training, and similar technologies.

catalyst deactivation, and complex reaction conditions. These limitations motivate the exploration of alternative degradation pathways that operate under mild conditions while avoiding added conventional catalysts like precious metals and avoiding external energy inputs. Contact electrification (CE) is a ubiquitous interfacial phenomenon arising from charge transfer during contact and separation of dissimilar materials [12–14]. Beyond its classical role in generating triboelectric charge for energy harvesting [15], CE has recently emerged as a previously underappreciated driving force for chemical reactivity at interfaces [16]. It was reported that sprayed microdroplets undergo H_2O_2 formation through hydroxyl $\cdot\text{OH}$ radicals recombination initiated by water-solid CE [17]. Furthermore, interactions between silicate surfaces and water vapor produce reactive oxygen species (ROS) over extended timescales, contributing to the chemistry to CE-induced charge transfer at gas/solid-water boundaries [18]. Moreover, triboelectrically charged polytetrafluoroethylene (PTFE) surfaces can generate highly energetic electrons capable of driving metal-ion reduction and electrochemiluminescent reactions, thereby establishing a direct link between CE and chemical transformation [19,20]. Building on this foundation, contact-electrocatalysis (CEC) emerges as a transformative strategy that harnesses charge transfer at solid-liquid interfaces CE to initiate and accelerate chemical reactions in aqueous [21,22] and nonaqueous [23,24] systems, including the redox reactions of $[\text{Fe}(\text{CN})_6]^{3-}/[\text{Fe}(\text{CN})_6]^{4-}$ couple, polymerization of aniline, fluorescence and luminescence reactions of terephthalic acid and luminol, and hydrogen peroxide production [21,25,26].

Compared with conventional AOPs or electrochemical approaches, CEC is initiated by CE at solid-liquid interfaces, associating with electron transfer and radical generation without external bias or metal electrodes, leading to spatially confined and interface-dominated reaction pathways. CE offers distinctive advantages, including broad material compatibility and intrinsic sustainability, highlighting its promise as a versatile platform for green and interfacial chemistry. In this work, we demonstrate that solid-liquid CE can directly induce the molecular-level degradation of BPB in aqueous solution. Through CE-driven interfacial electron transfer and radical generation, the robust aromatic and sulfone framework of BPB undergoes successive oxidative bond cleavage, leading to the formation of distinct low-molecular-weight fragments.

Through the integration of time-resolved UV–vis spectroscopy, high-resolution mass spectrometry and mechanistic analysis, the role of CEC in promoting efficient molecular breakdown of BPB is elucidated, without the need for external electrical input or oxidative catalysts. This work establishes a sustainable strategy for the degradation of persistent halogenated dyes and underscores the broader potential of CEC as a green platform for pollutant remediation and controlled molecular transformation.

2. Results and discussion

According to the electron cloud overlap mechanism, interfacial charge transfer in solid-liquid CE occurs when two surfaces approach sufficiently closely for the electron clouds of their surface atoms to overlap. Therefore, an effective CE-driven chemical system requires both (i) the construction of an intimate solid-liquid interface and (ii) sufficient mechanical input to enable frequent contact-separation events. In this work, the reaction system consists of an aqueous BPB solution and polytetrafluoroethylene (PTFE) powder, as schematically illustrated in Fig. 1a. The reaction is carried out in an ultrasonication bath equipped with a circulating cooling-water system. Continuous ultrasonic cavitation promotes repeated collision, contact, and separation between PTFE particles and the surrounding aqueous phase, thereby enhancing solid-liquid CE. Previous studies have shown that increasing ultrasonic power generally enhances cavitation intensity and collision frequency, leading to more efficient charge generation and accelerated degradation, whereas ultrasonic frequency influences bubble dynamics and contact times, thereby modulating the relative contributions of interfacial charge transfer and radical formation [27]. These considerations suggest that ultrasonic parameters provide an additional handle for tuning CEC efficiency and warrant systematic investigation in future studies. Importantly, the bath temperature is maintained at 25 °C throughout the experiment to exclude any contribution from thermal effects and to ensure that the observed reactions originate predominantly from CE-induced processes rather than heating.

To clarify the essential role of PTFE, a control experiment was conducted using a BPB solution subjected to ultrasonication in the absence of PTFE. As shown in Fig. S1, after 6 h of ultrasonication, the BPB

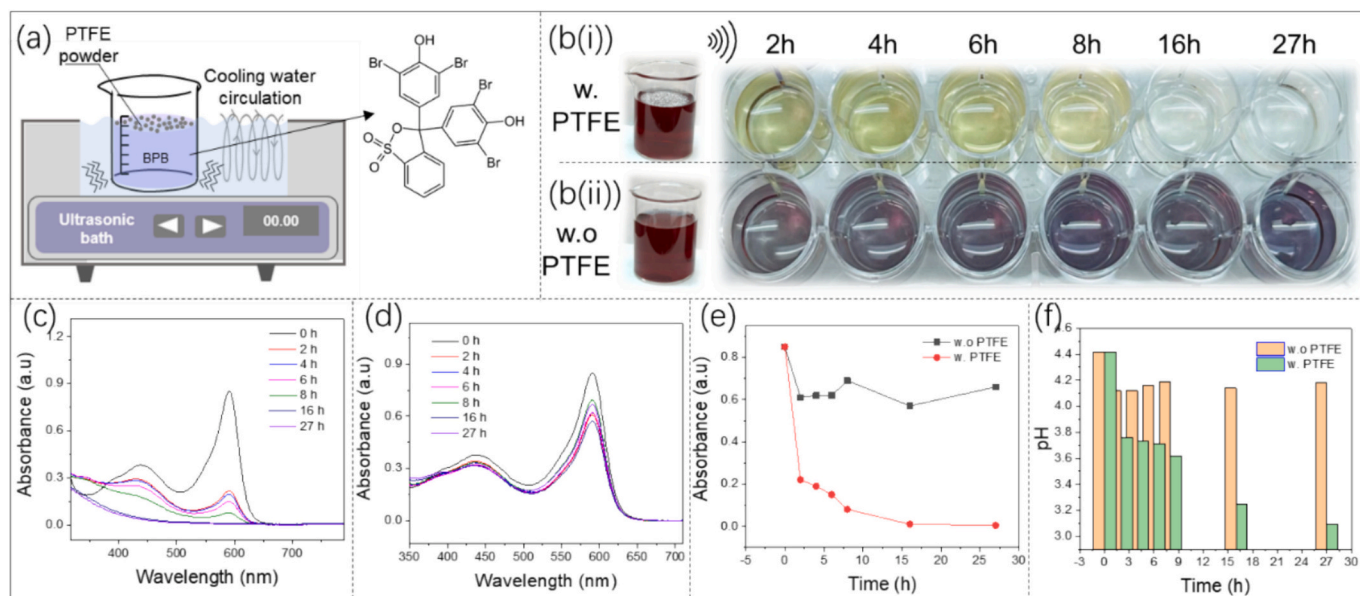


Fig. 1. (a) Schematic illustration of the experimental setup for BPB degradation using a PTFE-water interface under ultrasonication. (b) Photographs of BPB solutions with (upper row) and without (lower row) PTFE after different ultrasonication time intervals, showing the time-dependent color evolution. UV–vis absorption spectra of BPB solutions (0.2 mM) (c) with and (d) without PTFE collected at various ultrasonication time intervals. (e) Comparison of BPB degradation kinetics, expressed as the normalized absorbance at 590 nm, for solutions with PTFE (red line) and without PTFE (black line). (f) Time-dependent pH evolution of BPB solutions with and without PTFE during CEC. (For interpretation of the references to color in this figure legend, the reader is referred to the web version of this article.)

solution containing PTFE exhibited a clear color change from blue to yellow, whereas the BPB solution without PTFE showed almost no visible change. The time-dependent color evolution of the BPB solution with PTFE and without PTFE are further illustrated in Fig. 1b(i) and b(ii), respectively. In Fig. 1b(i), the solution initially appeared blue, gradually turned yellow after 2 h of ultrasonication, and became progressively lighter with increasing treatment time. After 16 h, the solution was nearly transparent, indicating substantial degradation of BPB. These visual observations are fully consistent with the UV-vis absorption spectra (Fig. 1c). The characteristic absorption peak of BPB at 590 nm decreased markedly with increasing ultrasonication time and nearly disappeared after 16 h in the presence of PTFE. In contrast, the photograph in Fig. 1b(ii) shows that the color of the BPB solution becomes only slightly lighter during the first 2 h of ultrasonication and then remains essentially unchanged even after 27 h in the absence of PTFE. Consistently, the characteristic absorption band of BPB under ultrasonication without PTFE exhibits only a minor decrease, which may be attributed to a weak sonochemical effect (Fig. 1d). [28] However, the persistent absorption intensity observed upon prolonged ultrasonication indicates that ultrasonication alone is insufficient to induce efficient BPB degradation [29,30]. Quantitative analysis of the absorbance at 590 nm (Fig. 1e) and the corresponding degradation efficiency (Fig. S2) further highlights the critical role of PTFE. In the presence of PTFE (red trace), the absorbance decreases from 0.85 to 0.22 within the first 2 h, corresponding to a degradation efficiency of approximately 74%, and reaches ~99% after 16 h of prolonged ultrasonication. By contrast, the BPB solution without PTFE shows only a ~28% decrease in absorbance during the first 2 h, followed by negligible further change upon extended ultrasonication. A similar trend is observed in the solution pH (Fig. 1f). In the presence of PTFE, the pH decreased significantly during ultrasonication, whereas only minor changes are observed without PTFE. This behavior is consistent with previous reported indicating that, caused by the large electronegativity difference between PTFE and water, electrons are transferred from water to the PTFE surface during CE, accompanied by the generation of protons, which leads to a decrease in solution pH [31,32]. Together, these results provide strong evidence that PTFE plays a decisive role in constructing an efficient solid-liquid CE platform that enables effective charge transfer and promotes BPB degradation.

In addition, the initial concentration of BPB significantly influences the CEC reaction rate. As shown in Fig. S3, a lower initial BPB concentration (0.1 mM) exhibited a more rapid decrease in the characteristic absorption peak than a higher concentration (0.2 mM), with the absorbance approaching zero within 6 h. This behavior can be attributed to the lower number of BPB molecules at reduced concentration, which facilitates more effective interaction between BPB molecules and the PTFE-water interface, thereby enhancing degradation efficiency. Moreover, the CEC-driven process achieves approximately 90.5% BPB (0.1 mM) degradation within 2 h, which is comparable the efficiencies reported for some established AOP or electrochemical systems (Table S1) [10,11,33,34]. More importantly, compared to these representative approaches, the CEC method reported here operates without external bias, electrodes, or added oxidants, highlighting its simpler operational requirements and potential for practical scalability.

BPB is a widely used acid-base indicator with an effective pH transition range of approximately 3.0–4.6, exhibiting a distinct color change from yellow under acidic conditions ($\text{pH} \approx 3.0$) to blue at higher pH values ($\text{pH} \approx 4.6$). Therefore, BPB was deliberately selected as a common organic dye pollutant with pH sensitive, allowing us to systematically explore the influence of solution pH on CEC-driven degradation under conditions relevant to real aqueous environments. By adjusting the initial pH of BPB solutions using sodium hydroxide, we were able to examine how different acid-base conditions affect degradation behavior in the CEC system. Notably, BPB is a weak acid, and its aqueous solution is inherently acidic upon dissolution ($\text{pH} = 4.41$), whereas neutral ($\text{pH} = 7.14$) and alkaline ($\text{pH} = 12.91$) conditions were achieved by adding

sodium hydroxide. As shown in Fig. S4, the UV-vis absorption spectra of BPB varied significantly with initial pH. Under acidic conditions, two main absorption bands were observed at approximately 440 nm and 590 nm. It has been well established that the absorption band near 440 nm corresponds to the acidic (yellow) form of BPB, whereas the band near 590 nm is characteristic of the basic (blue) form [11]. Notably, regardless of the initial pH, the absorption peak at ~590 nm is present in all cases. Therefore, in this study, the evolution of the ~590 nm peak is used as the primary metric to evaluate BPB degradation. For each pH condition, 15 mg of PTFE powder was added to the BPB solution, and all samples were subjected to identical ultrasonication conditions. Fig. 2a–c showed photographs of BPB solutions with different initial pH values, acidic ($\text{pH} = 4.41$), neutral ($\text{pH} = 7.14$), and alkaline ($\text{pH} = 12.91$), after various ultrasonication time intervals in the presence of PTFE. In all three cases, the solution color gradually faded with increasing ultrasonication time, indicating progressive BPB degradation. The corresponding UV-vis absorption spectra were shown in Fig. 2d–f. Under acidic conditions (Fig. 2d), as ultrasonication proceeds, the intensity of both absorption bands centered at approximately 440 nm and 590 nm decreased continuously, indicating effective degradation of BPB. For the neutral BPB solution (Fig. 2e), the absorption spectrum was dominated by a strong band at ~590 nm, consistent with the predominance of the blue form of BPB at near-neutral pH values. With increasing ultrasonication time, the intensity of this peak decreased monotonically, while the overall spectral profile remained similar, suggesting gradual degradation rather than a simple acid-base transformation. In the alkaline BPB solution (Fig. 2f), the initial absorbance at ~590 nm was significantly weaker than that under neutral conditions, reflecting differences in BPB speciation and molar absorptivity at high pH. Nevertheless, a clear time-dependent decrease in the 590 nm absorption band was still observed during ultrasonication, confirming that CEC remains effective even under strongly alkaline conditions. Overall, the consistent decrease in the characteristic absorption peak at ~590 nm across acidic, neutral, and alkaline environments demonstrated that the CEC approach enables BPB degradation over a broad pH range, despite substantial differences in initial BPB speciation and optical properties. According to the proposed CEC working mechanism, electron transfer from water to the negatively charged PTFE surface is accompanied by proton generation in the solution, leading to a decrease in the system pH [22]. Conversely, it has been reported that increased ionic concentration in the solution can inhibit solid-liquid contact electrification due to the formation of an interfacial electrical double layer (EDL), which screens interfacial charges and suppresses subsequent electron transfer [14,35]. As shown in Fig. S5, the BPB degradation efficiency is strongly pH-dependent, with the highest efficiency observed under acidic conditions without the addition of sodium hydroxide. The introduction of additional ions is therefore likely to influence the CEC process of BPB degradation. We suggest that increased ionic strength partially screens triboelectric charges on the dielectric surface via EDL formation, thereby inhibiting interfacial electron transfer and reducing degradation efficiency.

The working mechanism of CEC has been elucidated in numerous studies [36,37], involving interfacial charge transfer and the generation of ROS that subsequently attack and transform organic reactants. In this work, the degradation behavior of BPB under CEC conditions is schematically illustrated in Fig. 3a. When a solid dielectric such as PTFE undergoes repeated contact and separation with an aqueous phase, triboelectric charge transfer occurs at the interface, accompanied by the generation of $\cdot\text{OH}$ radicals and the accumulation of excess electrons on the PTFE surface. These accumulated electrons can subsequently be transferred to dissolved molecular oxygen, producing superoxide radicals ($\cdot\text{O}_2^-$) at the solid-liquid interface. The resulting ROS exhibit strong oxidative activity, driving the efficient degradation of BPB. In particular, Fig. S6 shows that the $\cdot\text{OH}$ radical signal detected by electron paramagnetic resonance (EPR) is significantly enhanced in the presence of PTFE compared to that observed in its absence. In addition,

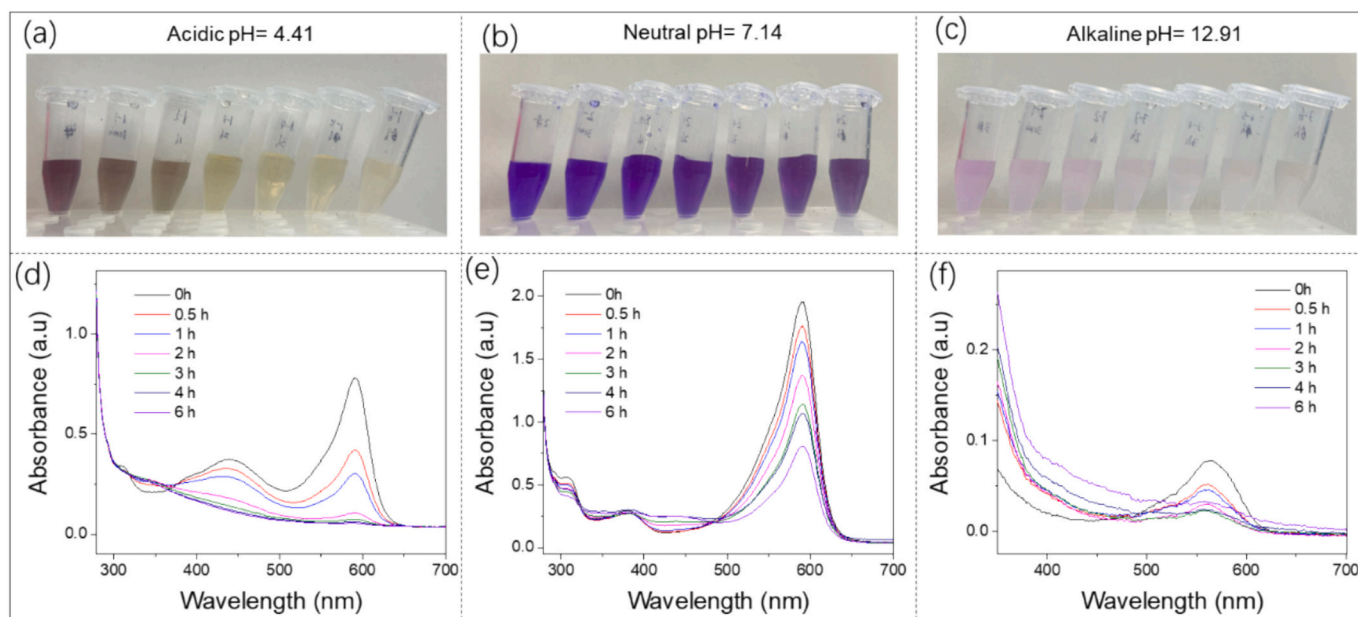


Fig. 2. Visual appearance (a-c) and corresponding UV-Vis absorption spectra (d-f) of BPB aqueous solutions during the CEC degradation process in the presence of PTFE powder at different initial pH values: acidic (pH = 4.41), neutral (pH = 7.14), and alkaline (pH = 12.91).

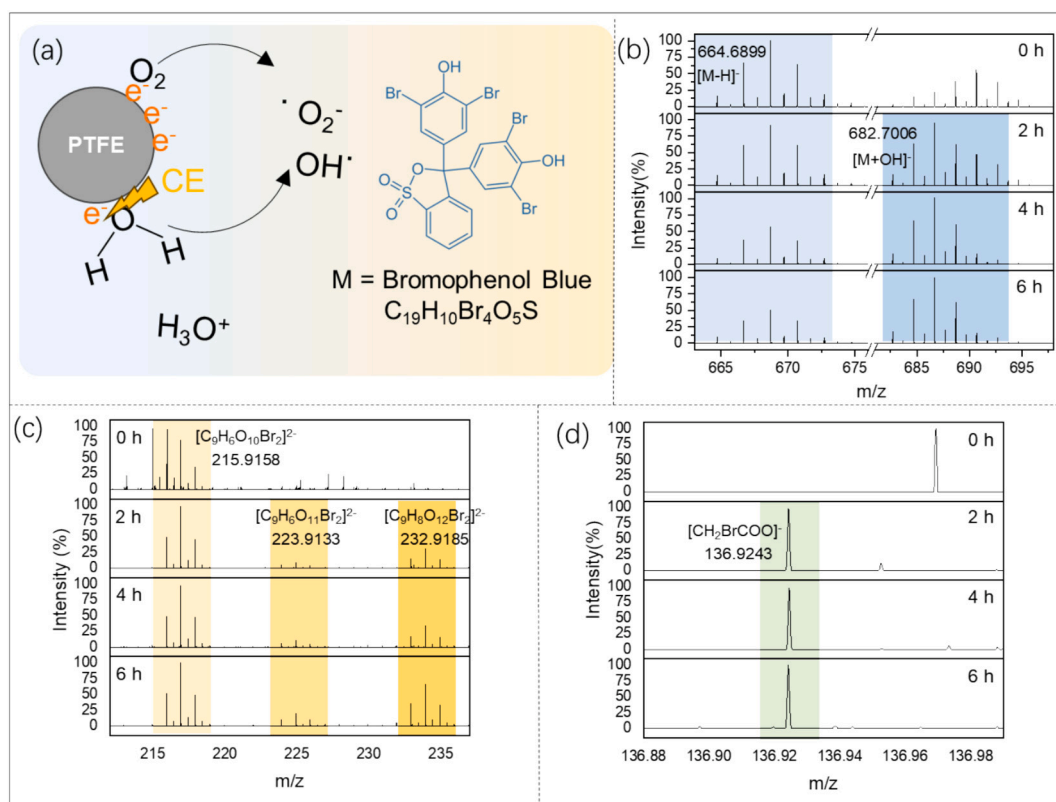


Fig. 3. (a) Schematic illustration of the proposed CEC mechanism for BPB degradation, highlighting interfacial charge transfer induced by contact electrification at the PTFE-water interface. (b, c) Representative intermediate products of BPB formed during the CEC degradation process, as detected by nESI-MS, illustrating the molecular transformation of BPB under CEC conditions.

nano-electrospray ionization mass spectrometry (nESI-MS) was employed to identify degradation intermediates, providing insight into the CEC reaction pathway. BPB features a highly conjugated sulfonaphthalein framework (see Fig. 1a) bearing multiple bromine substituents, which endows the molecule with pronounced resistance to

biodegradation and photolytic decomposition. Fig. 3b displayed the high- m/z region of mass spectrum under negative-ion ESI mode obtained during the different stages of BPB solution after CEC treatment. The dominant signal at $m/z = 664.6899$ is assigned to deprotonated BPB, $[M-H]^-$ (Fig. 3b, left blue panels), consistent with the molecular

formula $C_{19}H_{10}Br_4O_8S$. Moreover, the appearance of peak at $m/z = 682.6899$, corresponding to a + 18.0107 Da shift (Fig. 3b, right blue panels) relative to the parent $[M-H]^-$, might be assigned as $[M + OH]^-$. Fig. 3c showed the appearance of several signals in the m/z range of 215–235, which were assigned to doubly charged anions. This assignment is corroborated by the compressed m/z values and the halved isotopic spacing characteristic of multiply charged ions in high-resolution spectra. The detected ions, including $[C_9H_6O_{10}Br_2]^{2-}$ (m/z 215.9158), $[C_9H_6O_{11}Br_2]^{2-}$ (m/z 223.9133), and $[C_9H_6O_{12}Br_2]^{2-}$ (m/z 232.9185), indicate extensive molecular restructuring while preserving brominated aromatic subunits. The progressive increase in oxygen among these species strongly supports stepwise oxidative functionalization occurring prior to, or concomitant with, C–C bond cleavage of the parent sulfonephthalein framework. The retention of bromine isotopic patterns in these intermediates indicates that debromination is not the dominant initial pathway, consistent with reports that brominated aromatics typically undergo hydroxylation and ring activation prior to halogen loss during oxidative degradation [38–40]. The formation of stable dianions further suggests the presence of multiple acidic or strongly electron-withdrawing groups, such as phenolate and sulfonate moieties, which are known to promote multiply charged species in negative-mode ESI. Fig. 3d highlighted the emergence of a low- m/z fragment at m/z 136.9243, assigned to $[CH_2BrCOO]^-$. This ion is absent at 0 h and became prominent after CE treatment, indicating its origin from solution-phase chemical degradation rather than in-source fragmentation. The narrow peak width and reproducible intensity further support this conclusion. The formation of brominated acetic-acid-type fragments was consistent with advanced oxidative cleavage of aromatic rings, a pathway commonly observed in the degradation of halogenated dyes and phenolic compounds under radical-driven conditions. It was reported that the degradation likely proceeds via radical-initiated oxidation pathways, as previously reported for halogenated dyes under advanced oxidation conditions [10]. Upon exposure to CE-generated ROS [41,42], the electron-rich phenolic and aromatic moieties of BPB were preferentially attacked, leading to hydroxylation and oxidative activation of the molecular backbone. Moreover, phenol shares structural features with BPB and has been well established as a substrate that undergoes oxidative degradation mediated by $\cdot OH$ radicals [43]. Collectively, the MS results established a coherent degradation

sequence for BPB under CEC conditions: (i) hydroxylation of the intact molecule, (ii) formation of oxidized, bromine-retaining dianionic intermediates, and (iii) extensive fragmentation into low-molecular-weight carboxylates. Those observed mass shifts, charge states, and isotopic signatures are fully consistent with a radical-mediated oxidative degradation pathway initiated at the triboelectrically charged solid-liquid interface. Furthermore, structurally related aromatic dyes with conjugated backbones and electron-rich functional groups are therefore expected to undergo analogous interfacial oxidation pathways. In addition, the catalyst-free and interface-driven nature of CEC suggests potential applicability to broader classes of organic pollutants.

The electric-field catalysis framework developed by Shaik et al. and Ciampi et al. has demonstrated, both theoretically and experimentally, that oriented electric fields imposed by external bias can substantially lower reaction barriers, including those associated with C-halogen bond activation and C–Br bond activation at charged interfaces [44,45]. In this work, PTFE serve as a triboelectrically charged dielectric rather than a conventional electrode, and no sustained external circuit is involved. Instead, CE generates intense, localized interfacial electric fields at the PTFE-water interface, which may electrostatically stabilize polarized transition states and lower reaction barriers [46]. Moreover, the physical and chemical properties of the PTFE powder were systematically examined to confirm its structural and chemical stability, demonstrating that PTFE per se does not undergo reaction in the CEC process. Scanning electron microscopy (SEM) images of PTFE particles before and after CEC treatment in aqueous solution are shown in Fig. 4a. No discernible changes in particle morphology or surface features were observed, indicating that ultrasonication and repeated contact-separation cycles did not cause detectable physical damage to the PTFE powder. Elemental mapping analysis using energy-dispersive X-ray spectroscopy (EDS) further confirmed the compositional stability of PTFE (Fig. 4b). The spatial distribution and relative intensity of fluorine (F) signals remained unchanged before and after the CEC process, indicating that no fluorine loss or surface compositional alteration occurs during BPB degradation. Complementing the morphological analysis, spectroscopic techniques were employed to assess potential changes in the chemical structure of PTFE. Fig. 4c and d presented the Fourier transform infrared (FTIR) and Raman spectra, respectively, collected before and after CEC treatment. In the FTIR spectra, the characteristic absorption bands in the

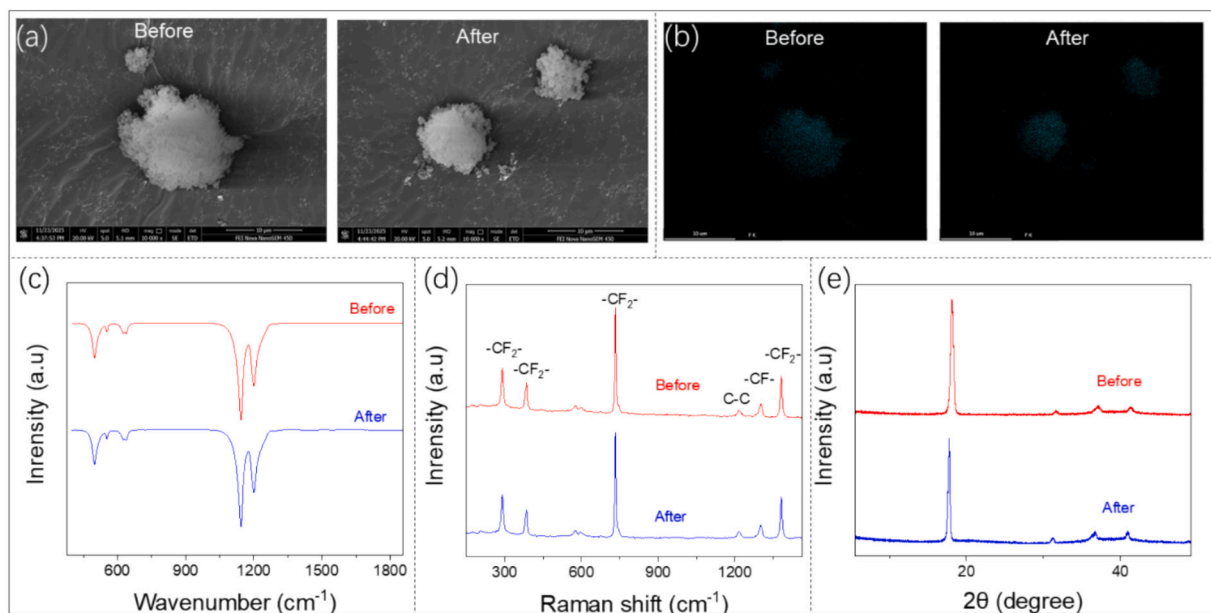


Fig. 4. Structural and chemical characterization of PTFE powder before and after the CEC treatment. (a) SEM images showing surface morphology, (b) corresponding EDS elemental mapping, (c) FTIR spectra, (d) Raman spectra, and (e) XRD patterns, collectively demonstrating the structural and chemical stability of PTFE during the CEC process.

fingerprint region below 1500 cm^{-1} remained unchanged, indicating the preservation of the C–F bonding environment. Similarly, Raman spectroscopy revealed identical skeletal vibration patterns for PTFE before and after the reaction, further confirming that the polymer backbone remains intact. Consistent with these observations, X-ray diffraction (XRD) patterns showed no detectable shift in diffraction peak positions or changes in peak profiles after the CEC process (Fig. 4e), indicating that the crystalline structure of PTFE remains intact despite ultrasonication and interfacial charge transfer. X-ray photoelectron spectroscopy (XPS) further probed the chemical states of PTFE before and after BPB degradation. The high-resolution C 1s and F 1s spectra (Fig. S7) revealed no shift in binding energies and no emergence of new peaks following the reaction. These results provide additional evidence that PTFE remains chemically stable and does not undergo surface chemical modification during CEC. Taken together, these results confirm that PTFE functions as a chemically inert and structurally stable solid dielectric, effectively mediating charge transfer without participating in chemical degradation or structural alteration.

3. Conclusion

In summary, we have demonstrated a CEC strategy free from the use of precious metal oxidative catalysts and without the application of any external electric fields for the efficient degradation of BPB in aqueous media. Continuous solid-liquid CE between PTFE powder and water under ultrasonication drives interfacial electron transfer and radical generation, enabling oxidative cleavage of BPB's chemically robust sulfonephthalein framework. Compared with conventional dye-degradation technologies such as electrode-based electrochemical oxidation or chemically intensive advanced oxidation processes, the CEC approach offers a conceptually simpler framework that operates without external power input, metal catalysts, or added oxidants, suggesting favorable prospects for scalable and low-maintenance implementation. By systematically examining BPB degradation across a wide pH range, this study demonstrates the general applicability of CEC under diverse aqueous conditions while revealing the coupled influence of ionic environment and interfacial electron transfer on degradation efficiency. Time-resolved UV–Vis spectroscopy, direct detection of CE-induced radicals, and nESI-MS collectively advance mechanistic understanding of CEC-driven transformations, including hydroxylation, formation of oxidized brominated intermediates, and subsequent fragmentation into low-molecular-weight species. Comprehensive morphological, structural, and spectroscopic analyses confirmed that PTFE remains chemically and structurally inert, functioning solely as a dielectric mediator for charge transfer. This work establishes CEC as a sustainable and versatile platform for the degradation of persistent halogenated dyes and highlights its broader potential for green interfacial redox reactions, pollutant remediation, and molecular transformation without reliance on external power sources or hazardous reagents.

4. Experimental section

About 15 mg of PTFE powder (Sigma-Aldrich, $10\ \mu\text{m}$) were added into a beaker containing 40 mL of as-prepared BPB (Sigma-Aldrich, Reagent, ACS) solution (0.2 or 0.1 mM) and stirred at 1000 rpm for 3 h. The reaction system was ultrasonicated (40 kHz, 120 W) in a certain time. The reaction temperature ($25\ ^\circ\text{C}$) was controlled by ultrasonic bath. The UV–Vis absorption spectra of samples were recorded with a Hitachi UV-4150 UV–Visible spectrometer on a range of 200–700 nm. The Scanning electron microscopy (SEM) images of the samples were obtained using an FEI Nova 450. The Energy Dispersive Spectroscopy (EDS) was conducted on FEI Nova 450 equipped with an AMETEK Octane Super appendix. FTIR spectroscopy was recorded on a Bruker Vertex 80 v on a range from 400 to 2000 cm^{-1} . The Raman spectroscopy was recorded on a LabRam HR evolution (HORIBA, SAS France), using a

range from 200 to 2000 cm^{-1} . The chemical states of PTFE before/after reaction were measured by near atmospheric pressure X-ray photoelectron spectrometer (NAP-XPS, SPECS, Germany). X-ray diffraction (XRD) of PTFE was measured using an advance diffractometer (Bruker-D8, Germany) with a working voltage of 40 kV. Hydroxyl radical for EPR analysis were prepared with 10.0 mL of DI water ultrasonication with PTFE, and 0.5 mL of 5,5-Dimethyl-1-pyrroline N-oxide (DMPO) was transferred to the solution during ultrasonication to capture radicals. An orbitrap mass spectrometer (MS) (LTQ XL Orbitrap, Thermo Fisher) was employed to detect species in the solution. The samples were introduced into MS by nano-electrospray ionization (nESI). A borosilicate glass capillary (B150–86–10, Sutter instrument, Novato, CA, USA) was pulled by a flaming/brown micropipette puller (P-87, Sutter instrument, Novato, CA, USA) to form two pieces of 3-cm length capillaries with tapered ends (ID: $3\ \mu\text{m}$). $10\ \mu\text{L}$ sample solution was then loaded from the open end (ID: 1.1 mm) of one capillary. When the capillary was mounted 2 mm in front of the MS inlet, a conductive needle was inserted from its open end and contacted with the liquid inside. A 1.5 kV high voltage was applied to the needle to trigger the spray ionization for the MS data recording.

CRedit authorship contribution statement

Shaoxin Li: Writing – original draft, Methodology, Investigation, Formal analysis, Data curation, Conceptualization. **Han Qian:** Methodology, Data curation. **Jinheng Xu:** Methodology, Data curation. **Zhong Lin Wang:** Supervision, Funding acquisition. **Richard N. Zare:** Writing – review & editing, Supervision, Funding acquisition. **Di Wei:** Writing – review & editing, Supervision, Funding acquisition, Conceptualization.

Declaration of competing interest

The authors declare that they have no known competing financial interests or personal relationships that could have appeared to influence the work reported in this paper.

Acknowledgement

D. W. acknowledges the National Natural Science Foundation (grant number 22479016) R.N.Z. acknowledges the Sustainability Accelerator Program of the Stanford Doerr School of Sustainability (GHG-0030-R.N.Z.)

Appendix A. Supplementary data

Supplementary data to this article can be found online at <https://doi.org/10.1016/j.jelechem.2026.119942>.

Data availability

Data will be made available on request.

References

- [1] R. Chavan, Health and environmental hazards of synthetic dyes, in: *Garment and Fashion Design at the University of Bahir Dar*, Bahir Dar, Ethiopia, 2013.
- [2] K. Singh, S. Arora, Removal of synthetic textile dyes from wastewaters: a critical review on present treatment technologies, *Crit. Rev. Environ. Sci. Technol.* 41 (2011) 807–878.
- [3] H. Ali, Biodegradation of synthetic dyes—a review, *Water Air Soil Pollut.* 213 (2010) 251–273.
- [4] A. Pastore, D. Badocco, L. Cappellin, P. Pastore, Modeling the dichromatic behavior of bromophenol blue to enhance the analytical performance of pH colorimetric sensor arrays, *Chemosensors* 10 (2022) 87.
- [5] V. Nand, M.J. Ellwood, A simple colorimetric method for determining seawater alkalinity using bromophenol blue, *Limnol. Oceanogr. Methods* 16 (2018) 401–410.

- [6] H. Zollinger, *Color Chemistry: Syntheses, Properties, and Applications of Organic Dyes and Pigments*, John Wiley & Sons, 2003.
- [7] R.G. Bates, *Determination of pH: Theory and Practice*, 1964.
- [8] J.-M. Zaldívar, J. Baraibar, A biology-based dynamic approach for the reconciliation of acute and chronic toxicity tests: application to *Daphnia magna*, *Chemosphere* 82 (2011) 1547–1555.
- [9] N. Bouanimba, R. Zouaghi, N. Laid, T. Sehili, Factors influencing the photocatalytic decolorization of bromophenol blue in aqueous solution with different types of TiO₂ as photocatalysts, *Desalination* 275 (2011) 224–230.
- [10] Q. Cong, M. Ren, T. Zhang, F. Cheng, J. Qu, Efficient photoelectrocatalytic performance of beta-cyclodextrin/graphene composite and effect of Cl⁻ in water: degradation for bromophenol blue as a case study, *RSC Adv.* 11 (2021) 29896–29905.
- [11] W. Li, B. Li, W. Ding, J. Wu, C. Zhang, D. Fu, Response surface methodology as a tool to optimize the electrochemical incineration of bromophenol blue on boron-doped diamond anode, *Diam. Relat. Mater.* 50 (2014) 1–8.
- [12] S. Lin, X. Chen, Z.L. Wang, Contact electrification at the liquid–solid interface, *Chem. Rev.* 122 (2021) 5209–5232.
- [13] Z. Wang, A. Berbille, Y. Feng, S. Li, L. Zhu, W. Tang, Z.L. Wang, Contact-electrocatalysis for the degradation of organic pollutants using pristine dielectric powders, *Nat. Commun.* 13 (2022) 130.
- [14] X. Li, Z.L. Wang, D. Wei, Iontronic logic control driven by dynamic electrical double layer regulation, *Iontronics* 1 (2025) 2.
- [15] X. Tao, T. Wang, L. Tan, F. Xu, A. Chen, Y. Yang, R. Zhang, X. Wang, High-performance constant current triboelectric Nanogenerator for wind energy harvesting and air purification, *SmartSys* 1 (2025) e70012.
- [16] X. Huo, S. Li, B. Sun, Z.L. Wang, D. Wei, Recent Progress of chemical reactions induced by contact electrification, *Molecules* 30 (2025) 584.
- [17] B. Chen, Y. Xia, R. He, H. Sang, W. Zhang, J. Li, L. Chen, P. Wang, S. Guo, Y. Yin, L. Hu, M. Song, Y. Liang, Y. Wang, G. Jiang, R.N. Zare, Water–solid contact electrification causes hydrogen peroxide production from hydroxyl radical recombination in sprayed microdroplets, *Proc. Natl. Acad. Sci.* 119 (2022) e2209056119.
- [18] Y. Xia, J. Li, Y. Zhang, Y. Yin, B. Chen, Y. Liang, G. Jiang, R.N. Zare, Contact between water vapor and silicate surface causes abiotic formation of reactive oxygen species in an anoxic atmosphere, *Proc. Natl. Acad. Sci.* 120 (2023) e2302014120.
- [19] C. Liu, A.J. Bard, Electrostatic electrochemistry at insulators, *Nat. Mater.* 7 (2008) 505–509.
- [20] C.-Y. Liu, A.J. Bard, Electrons on dielectrics and contact electrification, *Chem. Phys. Lett.* 480 (2009) 145–156.
- [21] K. Lee, S. Bose, X. Song, S.Q. Choi, R.N. Zare, Continuous flow contact electrocatalysis for hydrogen peroxide production, *J. Phys. Chem. C* 129 (2025) 6254–6261.
- [22] Z. Wang, X. Dong, W. Tang, Z.L. Wang, Contact-electro-catalysis (CEC), *Chem. Soc. Rev.* 53 (2024) 4349–4373.
- [23] T. Gan, Z. Yang, S. Li, H. Qian, Z. Li, J. Liu, P. Peng, J. Bai, H. Liu, Z. Wang, D. Wei, Unveiling Janus chemical processes in contact-electro-chemistry through oxygen reduction reactions, *J. Am. Chem. Soc.* 147 (2025) 25407–25416.
- [24] J. Liu, Z. Yang, S. Li, Y. Du, Z. Zhang, J. Shao, M. Willatzen, Z.L. Wang, D. Wei, Nonaqueous contact-electro-chemistry via triboelectric charge, *J. Am. Chem. Soc.* 146 (2024) 31574–31584.
- [25] S. Li, Z. Zhang, P. Peng, X. Li, Z.L. Wang, D. Wei, A green approach to induce and steer chemical reactions using inert solid dielectrics, *Nano Energy* 122 (2024) 109286.
- [26] C. Xu, S. Li, Z. Yang, M. Willatzen, Z. Lin Wang, D. Wei, Contact-electro-luminescence triggered by triboelectric charge, *Chem. Eng. J.* 501 (2024) 157754.
- [27] X. Dong, Z. Wang, A. Berbille, X. Zhao, W. Tang, Z.L. Wang, Investigations on the contact-electro-catalysis under various ultrasonic conditions and using different electrification particles, *Nano Energy* 99 (2022) 107346.
- [28] C.C.Y. Wong, J.L. Raymond, L.N. Usadi, Z. Zong, S.C. Walton, A.C. Sedgwick, J. Kwan, Enhancement of sonochemical production of hydroxyl radicals from pulsed cylindrically converging ultrasound waves, *Ultrason. Sonochem.* 99 (2023) 106559.
- [29] S.T. Muntaha, Z.L. Wang, D. Wei, Reevaluating mechano-driven chemical reactions: insights from ultrasonic, piezo, and contact-electro mechanisms, *Electrochim. Acta* 544 (2025) 147563.
- [30] S. Li, J. Liu, Z.L. Wang, D. Wei, Mechano-driven chemical reactions, *Green Energy Environ.* 10 (2025) 937–966.
- [31] Z. Tang, S. Lin, Z.L. Wang, Quantifying contact-electrification induced charge transfer on a liquid droplet after contacting with a liquid or solid, *Adv. Mater.* 33 (2021) 2102886.
- [32] Z.L. Wang, A.C. Wang, On the origin of contact-electrification, *Mater. Today* 30 (2019) 34–51.
- [33] T. Shah, T. Gul, K. Saeed, Photodegradation of bromophenol blue in aqueous medium using graphene nanoplates-supported TiO₂, *Appl Water Sci* 9 (2019) 105.
- [34] J. Kisala, A.M. Ferraria, N. Mitina, B. Cieniek, P. Krzemiński, D. Pogoćki, R. Nebesnyi, O. Zaichenko, Y. Bobitski, Photocatalytic activity of layered MoS₂ in the reductive degradation of bromophenol blue, *RSC Adv.* 12 (2022) 22465–22475.
- [35] J. Nie, Z. Ren, L. Xu, S. Lin, F. Zhan, X. Chen, Z.L. Wang, Probing contact-electrification-induced electron and ion transfers at a liquid–solid interface, *Adv. Mater.* 32 (2020) 1905696.
- [36] W. Li, J. Tu, J. Sun, Y. Zhang, J. Fang, M. Wang, X. Liu, Z.-Q. Tian, F. Ru Fan, Boosting reactive oxygen species generation via contact-electro-catalysis with FeIII-initiated self-cycled Fenton system, *Angew. Chem. Int. Ed.* 64 (2025) e202413246.
- [37] S. Li, Z.L. Wang, D. Wei, Chemical reactions at electrified interfaces, *Acc. Chem. Res.* 59 (2026) 285–297.
- [38] G.V. Buxton, C.L. Greenstock, W.P. Helman, A.B. Ross, Critical review of rate constants for reactions of hydrated electrons, hydrogen atoms and hydroxyl radicals ·OH/O⁻ in Aqueous solution, *J. Phys. Chem. Ref. Data* 17 (1988) 513–886.
- [39] U. von Gunten, Oxidation processes in water treatment: are we on track? *Environ. Sci. Technol.* 52 (2018) 5062–5075.
- [40] M.A. Oturan, J.-J. Aaron, Advanced oxidation processes in water/wastewater treatment: principles and applications. A review, *Crit. Rev. Environ. Sci. Technol.* 44 (2014) 2577–2641.
- [41] Z. Liang, W. Li, J. Tu, F.R. Fan, Mechanically induced contact-electro-catalysis: free radical generation, reaction pathways, and catalytic applications, *ChemCatChem* 17 (2025) e202500282.
- [42] J. Zhao, X. Zhang, J. Xu, W. Tang, Z. Lin Wang, F. Ru Fan, Contact-electro-catalysis for direct synthesis of H₂O₂ under ambient conditions, *Angew. Chem. Int. Ed.* 62 (2023) e202300604.
- [43] J. Xu, X. Song, Y. Lu, L. Lyu, C. Basheer, R.N. Zare, Intrinsic electric field triggers phenol oxidative degradation at microbubble interfaces, *J. Am. Chem. Soc.* 148 (2025) 43–49.
- [44] K. Dutta Dube, T. Stuyver, S. Kalita, S. Shaik, Solvent organization and rate regulation of a Menshutkin reaction by oriented external electric fields are revealed by combined MD and QM/MM calculations, *J. Am. Chem. Soc.* 142 (2020) 9955–9965.
- [45] M. Belotti, C. Hurtado, S. Kelly, M. MacGregor, N. Darwish, S. Ciampi, Toward the electrostatic catalysis of nucleophilic substitutions: a surface chemistry study of the Menshutkin reaction, *Langmuir* 40 (2024) 26633–26639.
- [46] Y. Wang, J. Zhang, W. Zhang, J. Yao, J. Liu, H. He, C. Gu, G. Gao, X. Jin, Electrostatic field in contact-electro-catalysis driven C–F bond cleavage of Perfluoroalkyl substances, *Angew. Chem. Int. Ed.* 63 (2024) e202402440.